Diagnostic and Interventional Imaging 102 (2021) 305–312

Original article/*Thoracic imaging*

Feasibility of lung imaging with a large field-of-view spectral photon-counting CT system

Salim Si-Mohamed[a,b,1,*], Sara Boccalini[a,b,1], Pierre-Antoine Rodesch[a], Riham Dessouky[a,c], Elias Lahoud[d], Thomas Broussaud[a], Monica Sigovan[a], Delphine Gamondes[b], Philippe Coulon[e], Yoad Yagil[d], Loïc Boussel[a,b], Philippe Douek[a,b]

[a] *Claude-Bernard University Lyon 1, CREATIS, CNRS UMR 5220, INSERM U1206, INSA-Lyon, 69621 Villeurbanne cedex, France*
[b] *Department of Radiology, Hospices Civils de Lyon, 69000 Lyon, France*
[c] *Department of Radiology, Faculty of Medicine, Zagazig University, 44519 Zagazig, Egypt*
[d] *Global Advanced Technologies, CT, Philips Research, 34900 Haifa, Israel*
[e] *Global Advanced Technologies, CT, Philips Research, 92000 Suresnes, France*

ARTICLE INFO

Keywords:
iDose
Lung
Phantoms
Photon-counting detector
Tomography, X-ray computed

ABSTRACT

Purpose: The purpose of this study was to characterize the technical capabilities and feasibility of a large field-of-view clinical spectral photon-counting computed tomography (SPCCT) prototype for high-resolution (HR) lung imaging.
Materials and methods: Measurement of modulation transfer function (MTF) and acquisition of a line pairs phantom were performed. An anthropomorphic lung nodule phantom was scanned with standard (120 kVp, 62 mAs), low (120 kVp, 11 mAs), and ultra-low (80 kVp, 3 mAs) radiation doses. A human volunteer underwent standard (120 kVp, 63 mAs) and low (120 kVp, 11 mAs) dose scans after approval by the ethics committee. HR images were reconstructed with 1024 matrix, 300 mm field of view and 0.25 mm slice thickness using a filtered-back projection (FBP) and two levels of iterative reconstruction (iDose 5 and 9). The conspicuity and sharpness of various lung structures (distal airways, vessels, fissures and proximal bronchial wall), image noise, and overall image quality were independently analyzed by three radiologists and compared to a previous HR lung CT examination of the same volunteer performed with a conventional CT equipped with energy integrating detectors (120 kVp, 10 mAs, FBP).
Results: Ten percent MTF was measured at 22.3 lp/cm with a cut-off at 31 lp/cm. Up to 28 lp/cm were depicted. While mixed and solid nodules were easily depicted on standard and low-dose phantom images, higher iDose levels and slice thicknesses (1 mm) were needed to visualize ground-glass components on ultra-low-dose images. Standard dose SPCCT images of in vivo lung structures were of greater conspicuity and sharpness, with greater overall image quality, and similar image noise (despite a flux reduction of 23%) to conventional CT images. Low-dose SPCCT images were of greater or similar conspicuity and sharpness, similar overall image quality, and lower but acceptable image noise (despite a flux reduction of 89%).
Conclusions: A large field-of-view SPCCT prototype demonstrates HR technical capabilities and high image quality for high resolution lung CT in human.

1. Introduction

During the past five years, a new generation of computed tomography (CT) devices equipped with energy-resolved photon-counting detectors (PCDs) has emerged with promising results for various preclinical and clinical applications [1–3]. These initial studies have focused on imaging tasks that could benefit from high-resolution (HR) and lower radiation dose capabilities such as lung imaging [4–6].

Abbreviations: CT, Computed tomography; $CTDI_{vol}$, Volume CT dose index; EID, Energy-integrating detectors; FOV, Field-of-view; HR, High-resolution; HU, Hounsfield unit; MTF, Modulation transfer function; PCD, Photon-counting detector; SPCCT, Spectral photon-counting computed tomography.

* Corresponding author at: Claude-Bernard University Lyon 1, CREATIS, CNRS UMR 5220, INSERM U1206, INSA-Lyon, 69621 Villeurbanne cedex, France.
E-mail address: salim.si-mohamed@chu-lyon.fr (S. Si-Mohamed).
[1] First author with equal contribution.

https://doi.org/10.1016/j.diii.2021.01.001
2211-5684/

Compared to energy integrating detectors (EIDs) used in conventional and dual-energy CT systems, PCD technology takes advantage of the absence of scintillators, which require reflective layers between detector pixels [3,7]. This minimizes pixel size and maximizes spatial resolution. PCDs also use a direct conversion technology counting the photons incoming into detector pixels and sorting them into several energy bins. This suppresses electronic noise inside the readout circuit of each pixel by setting energy thresholds over the noise values (around 20–25 keV) [8]. Due to multiple energy bins, SPCCT systems can provide both conventional and material decomposition images as with dual-energy systems [9,10] but with the additional value of K-edge imaging of high atomic number materials, known as material specific quantitative imaging [1,11–15].

While EIDs only measure the amount of energy deposited in each pixel due to an indirect conversion that boosts the weight of high-energy photons, PCDs measure the photon counts per bin. The energy weighting of the lower energy photons is consequently more important in PCDs. This effect leads to higher tissue contrast since material attenuation depends on the energy with an increase in photoelectric attenuation coefficient towards the lower energy spectrum (~30–40 keV) [7]. These technical features may explain why SPCCT technology holds the promise of being the next-generation of CT systems. Nevertheless, these systems still have limitations, such as field-of-view (FOV), detector array size, and count rates. In an attempt to overcome these current limitations, a large FOV SPCCT prototype has been built.

The purpose of this study was to characterize the technical capabilities and feasibility of a large FOV clinical SPCCT prototype in HR lung imaging.

2. Material and methods

2.1. SPCCT system

A large FOV (500 mm in-plane) clinical prototype system (Philips Healthcare) equipped with energy-sensitive PCDs of 2-mm-thick cadmium zinc telluride with a pixel pitch of $270 \times 270\ \mu m^2$ at isocenter, bonded to Philips' proprietary ChromAIX2 application-specific integrated circuit, relying on the direct conversion high band gap semiconductor of cadmium zinc telluride was used for this study [16]. Each channel offered pulse-height discrimination with five controllable energy thresholds from 30 to 120 keV. The full spectral image chain followed a two-step approach for reconstruction. The photon counts from the five energy bins were used to provide conventional CT images. For each pixel, a maximum likelihood estimator was used to derive an equivalent water-thickness per pixel from the photon counts in the five energy bins. Conventional images were then reconstructed from the water-thickness equivalent sinograms using a filtered-back projection algorithm. A photograph of the system and schematic representation of the photon-counting measurement process is given in Fig. 1. Further technical details are provided in Table 1.

Table 1
System parameters of the clinical prototype spectral photon counting computed tomography (SPCCT) system.

Parameter	SPCCT
Platform	Philips iCT
Supported scan modes	Axial, Axial multicycles, Helical
Tube voltages [kVp]	80, 100, 120, 140
Tube currents [mA]	10–500
X-ray filter	Half value layer HVL = 7.1 ± 0.7 mm at 120 kVp
Focal spot [mm × mm]	0.6 × 0.7 (dual focal spots)
Gantry rotation [s]	0.33, 0.4, 0.5, 0.75, 1.0
Projections per rotation	2400
Number of focal spots	2
Z-coverage in isocenter [mm]	17.5
Number of detectors per row/column	64/1848
Field-of-view [mm]	500
Pixel pitch [μm × μm]	274 × 274 mm^2 at isocenter
Readout electronic	Philips ChromAIX2
Number of energy thresholds	5
Sensor material	Cadmium Zinc Telluride, 2 mm thickness

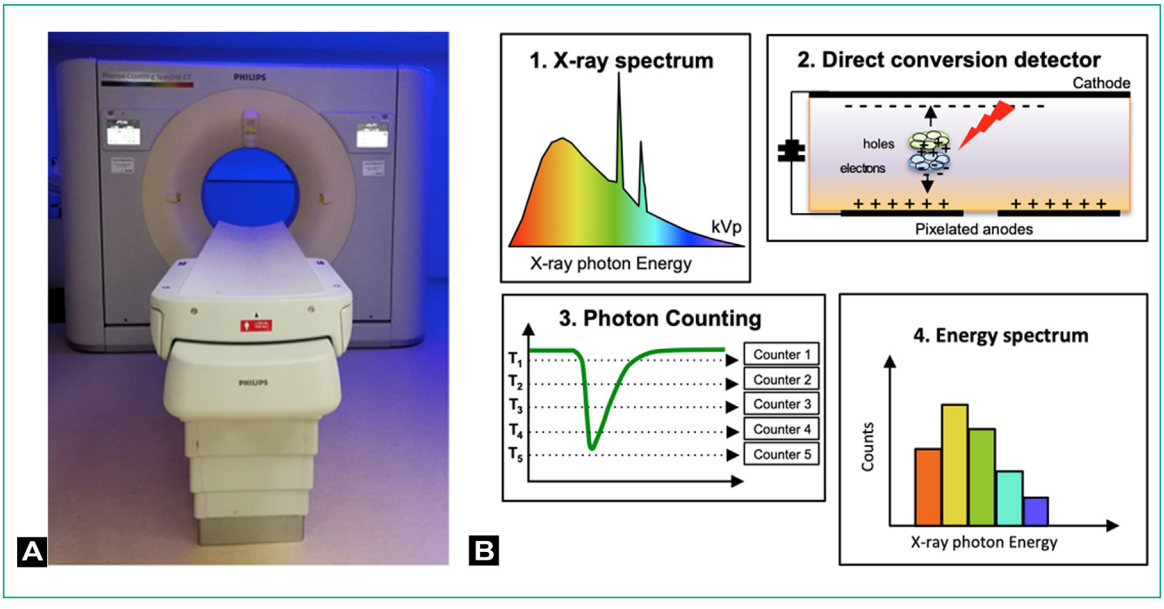

Fig. 1. A. Spectral photon-counting computed tomography prototype system. B. Schematic representation of the photon-counting measurement process. Each individual X-ray interacting in the semiconductor detector is creating electron-hole pairs. The number of pairs is directly proportional to the X-ray energy. High voltage applied to the electrodes allows collecting the charges in an electric pulse with intensity proportional to the X-ray energy. Multiple thresholds allow classifying each X-ray according to its energy.

2.2. Phantom experiments

2.2.1. Spatial resolution imaging

In order to assess the in-plane spatial resolution, a phantom with a 20 cm epoxy interior and solid water shell containing a 50 μm tungsten wire positioned 15 mm off the isocenter (slice sensitivity and geometric evaluation module, advanced iqModules™, Gammex) was scanned in the axial mode at 120 kVp, 200 mAs. The resolution was evaluated quantitatively using the modulation transfer function (MTF). Conventional images, representing a region-of-interest around the wire were reconstructed with a 60 mm FOV, matrix size of 2048, and a slice thickness of 0.275 mm [voxel size at 0.029 (x) × 0.029 (y) × 0.275 (z) mm^3] using a PCD adapted high-resolution back-projection filter (filter Detailed 1). The reconstructed images were analyzed using an in-house Matlab tool that produced the radial profile obtained from averaging several slices and derived the MTF curve by Fourier transform of the radial profile with compensation for the finite wire diameter. In addition, a subjective evaluation of a line pair phantom (high-contrast resolution module, advanced iqModules™, Gammex), scanned in axial mode at 120 kVp, 200 mAs was performed. This module features line pairs with resolutions up to 32 lp/cm. The phantom was scanned in different positions so that each acquisition focused on 1 module of interest placed 15 mm off its isocenter. Conventional images were reconstructed with the same parameters previously described.

2.2.2. Lung nodule imaging

An anthropomorphic lung phantom (QRM-lung nodule phantom, GmbH) housing two types of spherical nodules (*i.e.*, a subsolid one with mixed density [shell: −795 Hounsfield unit (HU), center: 50 HU at 120 kVp] and a second solid one [20 HU at 120 kVp]), was scanned using different radiation doses. The phantom had a water equivalent diameter of 21.3 cm, corresponding to a standard size patient chest. Helical acquisitions were performed with standard (120 kVp, 62 mAs), low (120 kVp, 11 mAs), and lowest possible scanner setting equivalent to an ultra-low-dose protocol (80 kVp, 3 mAs) with a 1.03 pitch value and 0.33 s rotation time. Images were reconstructed with a 300 mm FOV, a 1024 matrix size, and 0.250 mm slice thickness and an appropriate (detailed 2) filter.

2.3. HR human lung imaging

HR lung images of a 60-year-old man with body mass index of 30 kg/m^2 were acquired under the authorization of the local ethics committee (protocol number: 2018-A02696-49). Standard (120 kVp, 63 mAs) and low-dose (120 kVp, 11 mAs) lung imaging was performed. This volunteer had undergone a previous standard dose (120 kVp, 103 mAs) high-resolution lung CT in our institute using a conventional CT system (Brilliance 64; Philips Healthcare) that allowed for image quality comparison. Images were reconstructed with a 1024 matrix, a 300 mm FOV and a 0.25 mm slice thickness using filtered-back projection and two levels of hybrid iterative reconstruction algorithm (iDose level 5 and 9) adapted for photon-counting data. Acquisition and reconstruction parameters are summarized in Table 2.

A subjective comparison of image quality between conventional CT and SPCCT images reconstructed with a filtered-back projection algorithm was performed independently by three independent readers (D. G., S. B., S. S.-M., with 15-, 6- and 6 years of experience in lung imaging, respectively) on a clinical workstation. Each reader rated the conspicuity and sharpness of different lung structures (distal airways, fissure, distal vessels, proximal bronchial wall), the subjective image noise using a 5-point Likert scale (1: unacceptable, 2: suboptimal, 3: acceptable, 4: above average, 5: excellent) and the overall image quality using a 4-point Likert scale (1: not evaluable, 2: interpretable despite moderate artefact or noise, 3: fully interpretable with mild artifacts or noise, 4: fully interpretable with no artifacts or noise). Objective image noise was measured in a 40 mm^2 region-of-interest drawn in a peripheral aerated portion of the lung.

2.4. Radiation dose

Tube current, tube voltage and volumetric CT dose index ($CTDI_{vol}$) were recorded. Due to a smaller z-axis collimation and consequent over-beaming (penumbra) compared to conventional CT, the SPCCT prototype has a greater $CTDI_{vol}$ for the same tube voltage and current parameters. This consequent off-collimation radiation dose does not contribute to the image quality, but only to the $CTDI_{vol}$. This means that a fair comparison between protocols has to be performed using the same acquisition parameters (*e.g.*, the X-ray flux or total number of photons emitted by the X-ray tube) that is determined by mAs, kVp, system geometry, and tube filtration. Because of different X-ray filtration between the systems used in the present study, the flux of SPCCT was ∼25% greater at same mAs than with conventional CT. Effective dose was estimated from the product of the dose length by the normalised effective dose conversion coefficient of 0.014 $mSv.mGy^{-1}.cm^{-1}$ [17].

2.5. Statistical analysis

Image quality rating was averaged among the three readers and data were expressed as mean values.

3. Results

3.1. Phantom experiments

3.1.1. Spatial resolution imaging

Mean spatial resolutions were measured at 11.6 and 22.3 lp/cm at 50% and 10% MTF respectively, with a cut-off at 31 lp/cm (Fig. 2A). Visual evaluation of the line pair phantom allowed visualization of up to 28 lp/cm, corresponding to a line width of 178 μm (Fig. 2B).

3.1.2. Lung nodule phantom imaging

The borders of both nodules as well as the ground glass portion of the subsolid nodule were well defined at 62 mAs ($CTDI_{vol}$ at 6.65 mGy) (Fig. 3). With the low-dose protocol at 11 mAs ($CTDI_{vol}$ at 1.11 mGy), the margins appeared less defined but nodules were clearly depicted nonetheless. With the ultra-low-dose protocol at 80 kVp and 3 mAs ($CTDI_{vol}$ at 0.10 mGy), the ground glass portion was more difficult to distinguish from background noise. In this case, the use of iDoses 5 and 9 improved border and ground glass opacity visualization (Fig. 3).

3.2. HR human lung imaging

Table 3 shows the subjective image quality analysis of HR lung imaging on conventional and SPCCT systems (Figs. 4 and 5). Conspicuity and sharpness of distal airways, fissures, distal vessels and proximal bronchial wall were greater on standard dose SPCCT images (mean score of 4 or 5). Despite a tube flux reduction of 23% for standard dose SPCCT images, overall image quality was greater on SPCCT images (mean score of 4 *vs.* 3) compared to conventional CT images. Despite greater matrix size and smaller slice thickness of standard dose SPCCT images, noise values were equivalent (83.2 HU *vs.* 82.5 HU, respectively), while subjective noise quality was greater (mean score of 5 *vs.* 3.7, respectively) than conventional CT images. Conspicuity and sharpness of distal airways, fissures, distal vessels and proximal bronchial wall were either similar or greater on low-dose SPCCT images, (mean score of 3 or 4). Despite

Table 2
Acquisition and reconstruction parameters for conventional and spectral photon-counting computed tomography (SPCCT) imaging.

	Standard dose SPCCT	Low dose SPCCT	Ultra-low dose SPCCT	Standard dose conventional CT
Acquisition parameters				
Tube voltage (kVp)	120	120	80	120
Tube current (mAs)	62	11	3	103
Rotation time (s)	0.75	0.75	0.33	0.50
Pitch	1.03	1.03	1.03	0.89
Mode	Helical	Helical	Helical	Helical
Reconstruction parameters				
Field-of-view (mm)	300	300	300	300
Matrix	1024	1024	1024	512
Slice width (μm)	250	250	1000	800
Reconstruction method	FBP, iDose 5–9	FBP, iDose 5–9	FBP, iDose 5–9	FBP
Filter	Detailed 2	Detailed 2	Detailed 2	YA

FBP: filtered-back projection; SPCCT: spectral photon-counting computed tomography.

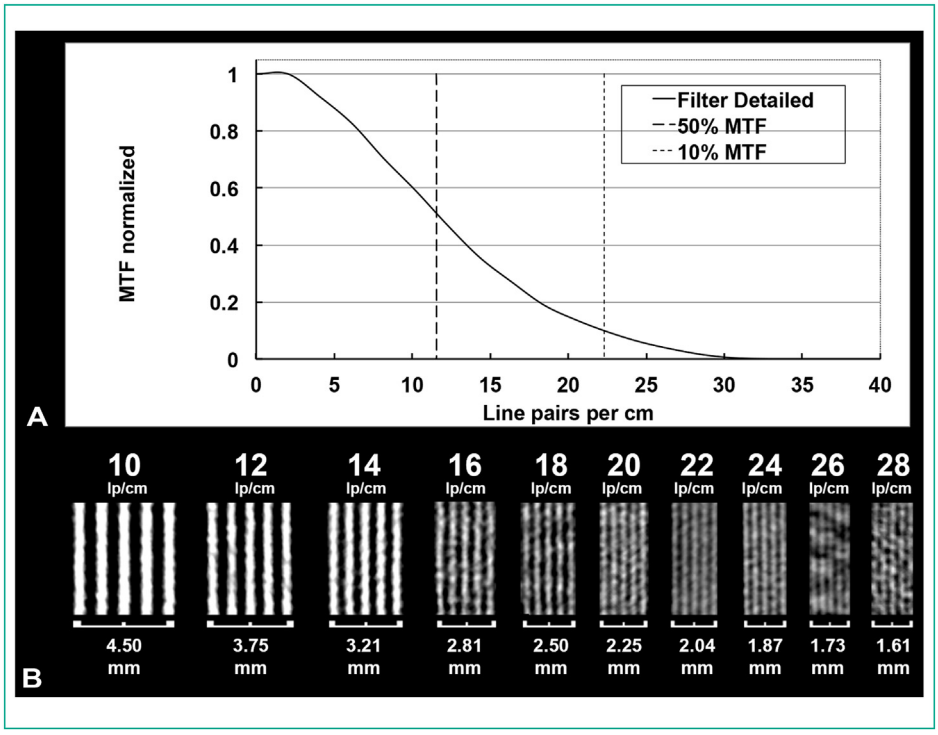

Fig. 2. Spectral photon-counting computed tomography key features imaging of spatial resolution. A. Average modulation transfer functions across slices for the 50 μm tungsten wire scanned at 15 mm from isocenter (reconstruction parameters: 2048 matrix size, 60 mm field of view, filter detailed 1, 0.275 mm slice thickness). B. Images with a voxel size at 0.029 (x) × 0.029 (y) × 1.1 (z) mm^3 of high-contrast resolution module focused on visualization of 5 dense lines. Detectability of line pairs is possible up to 28 lp/cm (corresponding to a line thickness at 178 μm).

a tube flux reduction of 87% between low-dose SPCCT and standard dose conventional CT images, overall image quality was equivalent among both images (mean score of 3). Image noise was greater on low-dose SPCCT images compared to standard dose conventional CT images (142.7 HU *vs.* 82.5 HU), but subjective image quality remained acceptable (mean score of 3). The addition of iDose to SPCCT images decreased noise values by about 35% with iDose 5 and 68% with iDose 9 and changed the noise texture as expected from iterative reconstruction. Image quality was not rated, but all readers agreed that the conspicuity and sharpness of the lung structures were preserved with the added benefit of noise reduction (Fig. 4).

4. Discussion

High-resolution CT imaging is necessary for various clinical applications in the lung such as parenchymal and interstitial tissue, distal airway and vessel assessment [18–23]. In this study, we showed the high capabilities of high-resolution large FOV SPCCT prototype for these tasks. We found that it is possible to visualize up to 28 lp/cm on a line pair phantom. Feasibility of solid and mixed nodules depiction has been shown under standard, low and ultra-low radiation doses. Finally, image acquisition from a human volunteer demonstrated high image quality compared to conventional CT even with lower radiation dose.

SPCCT technology represents a breakthrough in CT imaging because of the new PCDs. Their architectural features allow a much smaller pixel size (around 100–500 microns) than EIDs [3,7,8]. Furthermore, PCD manufacturers have decreased the area of each detector pixel to minimize the count rate per pixel, avoiding loss of photon counts and mis-registration of photon energy occurring at high count rates [3,7]. This is of interest for spatial resolution capabilities. An additional feature of PCDs is the higher dose efficiency owing to electronic noise suppression. This is explained by the energy-resolving characteristics that detect and measure

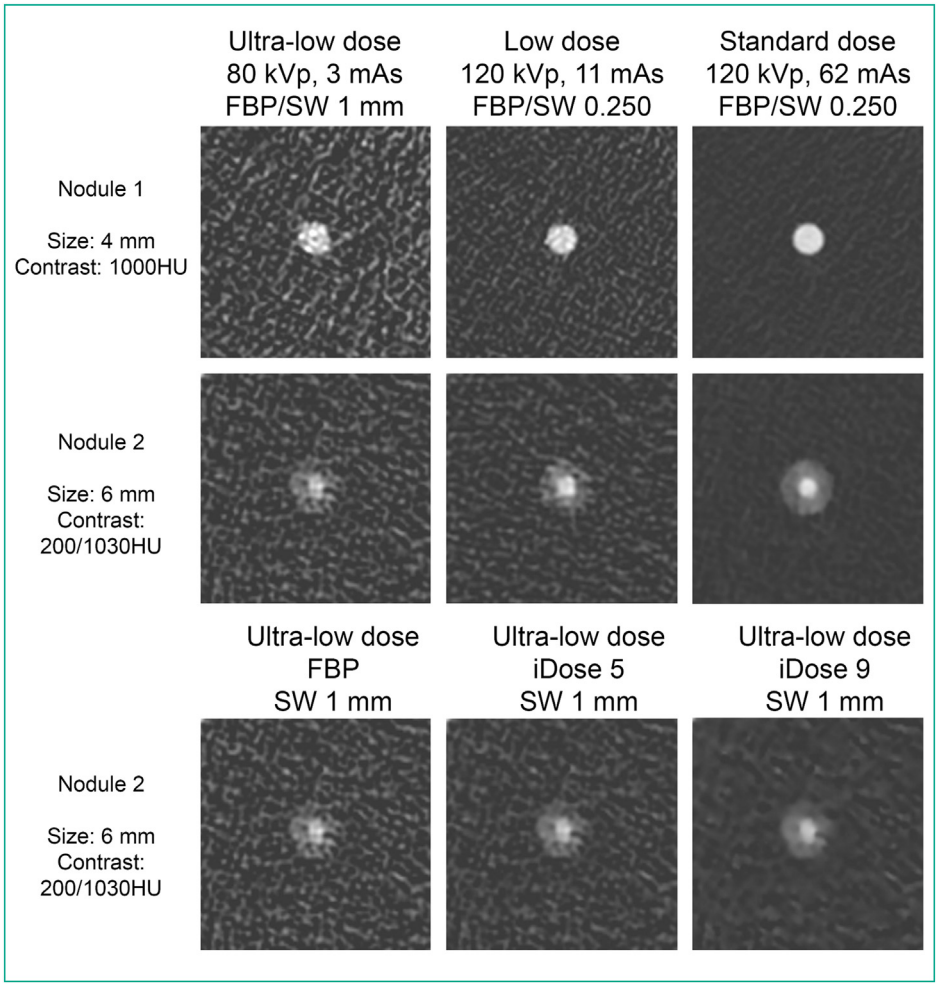

Fig. 3. High matrix spectral photon-counting computed tomography (SPCCT) standard, low and ultra-low-dose imaging of lung nodules. Imaging characteristics of different nodules scanned with the SPCCT system (WL, −600 HU, WW, 1600 HU). Images were acquired with different radiation dose (ultra-low-dose, low-dose, standard dose) and reconstructed with filtered-back projection (FBP) and iterative reconstruction (iDose 5 and 9 for ultra-low-dose imaging). Reconstruction parameters: first and second row: first column: FOV, 300 mm; matrix, 1024; SW, 1 mm; filter, detailed 2; FBP. Second column: FOV, 300 mm; matrix, 1024; SW, 0.250 mm; filter, detailed 2; FBP. Third column: FOV, 300 mm; matrix, 1024; SW, 0.250 mm; filter, detailed 2; FBP. Third row: FOV, 300 mm; matrix, 1024; SW, 1 mm; filter, detailed 2; FBP; iDose, level 5 and 9.

Table 3
Subjective image analysis of conventional and spectral photon-counting computed tomography (SPCCT) human lung imaging.

	Standard dose conventional CT	Standard dose SPCCT	Low dose SPCCT
Overall image quality	3	4	3
Noise image quality	3.7	5	3
Distal airways			
Conspicuity	3	5	2.7
Sharpness	2	4.3	2.7
Fissures			
Conspicuity	2.7	5	2.7
Sharpness	2	4.3	3
Proximal bronchial wall			
Conspicuity	3	5	4
Sharpness	3	5	3
Distal vessels			
Conspicuity	2.5	5	4
Sharpness	2.3	5	3.3

Data are expressed as mean score of the three different readers scores. Overall image quality was rated using a 4-points Likert scale (1: not evaluable, 4: fully interpretable with no artifacts or noise). Noise and lung structures image quality were rated using a 5-points Likert scale (1: unacceptable, 5: excellent).
SPCCT: spectral photon-counting computed tomography.

electronic noise as photons of low-energy (around 20–25 keV). By fixing the lower threshold of detection at a value higher than this energy range (*e.g.*, 30 keV on the current system), the electronic noise will not be recorded [3,7,8]. These key features explain the potential of SPCCT technology in HR lung imaging as highlighted in this study. First, MTF performance was reported 10% at 22.3 lp/cm with a cut-off at 31 lp/cm. Evaluation of a line pair phantom depicted a 178 μm line width which is in line with photon-counting detector expectations [4,24,25]. Despite the high performance and because of intrinsic limitations of MTF evaluation (*e.g.*, high radiation dose with a high-contrast object), a subjective analysis remains mandatory using standard clinical protocols. Second, in vitro lung nodule imaging demonstrated excellent image quality under standard radiation dose. This has been previously demonstrated with a limited FOV SPCCT from the same manufacturer [26]. Third, image quality in a human volunteer was rated excellent by three experienced lung radiologists. The image noise was excellent with a particular texture that characterizes high frequency noise, such as expected with PCDs [7]. Small lung structures such as distal airways and vessels, bronchial wall and fissures were also depicted with high quality, such as suggested previously using a limited FOV SPCCT from a different manufacturer [26]. Finally, comparison between SPCCT and conventional CT images demonstrated a

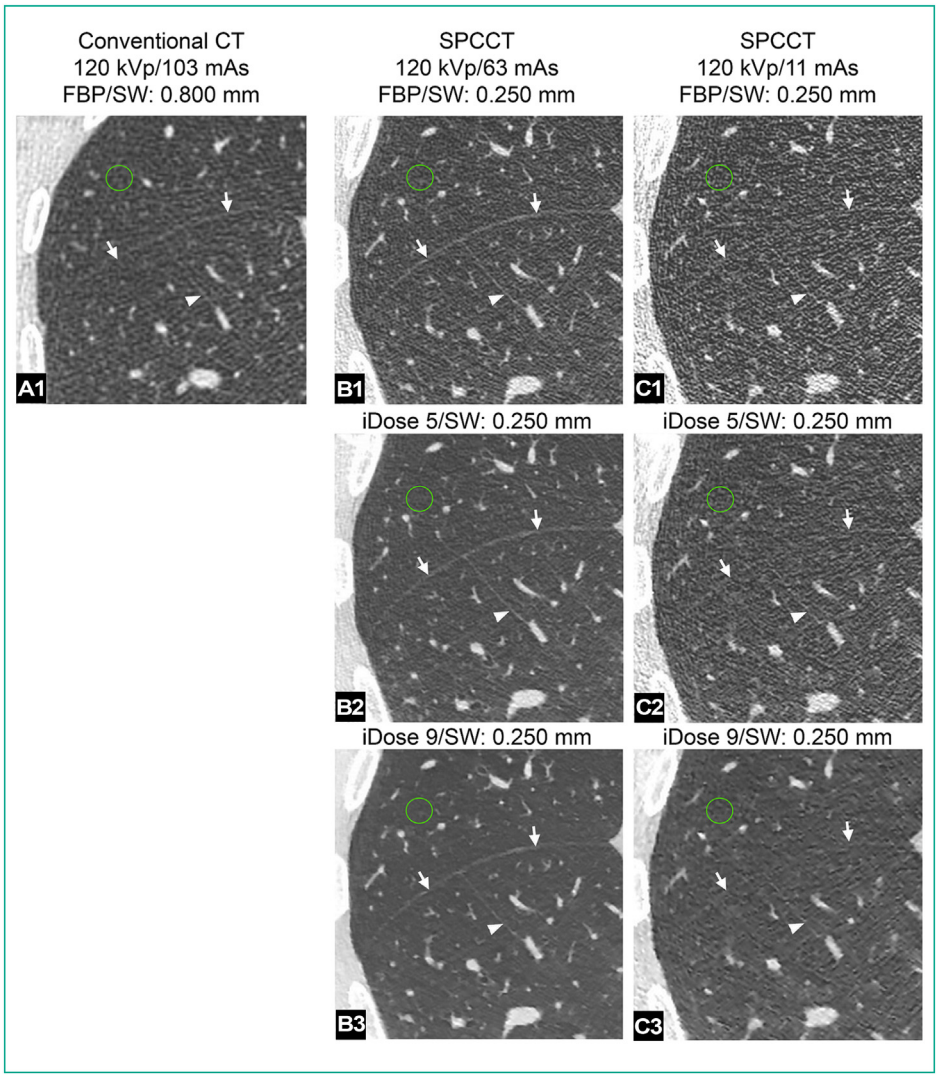

Fig. 4. Human high-resolution spectral photon-counting computed tomography (SPCCT) lung imaging (high matrix, small slice width) as compared to a conventional CT: low-dose and iterative reconstructions (WL −600 HU, WW 1600 HU). The small fissure (arrows) and an accessory fissure of the right inferior lobe (arrowheads) are shown on three acquisitions of the same subject obtained with a Brilliance 64 CT system (A, 120 kVp; 103 mAs; CTDIvol: 6.1 mGy; equivalent dose: 1.87 mSv) and with the SPCCT system (B and C) at standard (B, 120 kVp; 66 mAs; CTDIvol: 6.65 mGy; equivalent dose: 2.00 mSv) and low-dose (C, 120 kVp; 11 mAs; CTDIvol: 1.11 mGy; equivalent dose: 0.33 mSv), respectively. These structures are better depicted on the SPCCT acquisition at 66 mAs (B1) compared to a conventional CT image (A) notwithstanding the higher dose of the latter. The fissures are also visible on the low-dose SPCCT acquisition (C) even if the background noise is increased. Note that the SPCCT images are at significantly narrower slice thickness: 0.250 mm as opposed to 0.800 mm in the Brilliance 64 CT image. B1–B3 show the same image obtained with SPCCT (120 kVp and 66 mAs) and reconstructed with filtered-back projection (B1), iDose level 5 (B2) and iDose level 9 (B3). C1–C3 show the same image obtained with low-dose SPCCT (120 kVp and 11 mAs) and reconstructed with filtered-back projection (C1), iDose level 5 (C2) and iDose level 9 (C3). Noise values were measured for each acquisition within the regions-of-interest shown in green in the images. Reconstruction parameters: A – matrix, 512; slice thickness, 0.800 mm; kernel YA. B1–B3 and C – matrix, 1024; slice thickness, 0.250 mm; filter, detailed 2.

greater conspicuity and sharpness of various small lung structures and a greater overall image quality on SPCCT images among all subjective image readers, confirming the results from a recent study using a different limited FOV SPCCT system [6]. Furthermore, a greater subjective noise quality and similar noise values were found despite different acquisition (flux reduction of 23%) and reconstruction (1024 matrix, 0.25 mm slice thickness) parameters known to result in increased noise values. Nevertheless, these reconstruction parameters were chosen to convey the intrinsic spatial resolution of PCDs.

Another feature highlighted in this study is dose efficiency. First, we have shown the feasibility of an ultra-low-dose lung imaging (80 kVp, 3 mAs) for depiction of solid and mixed nodules while maintaining a matrix size at 1024 mm and a high frequency filter. Solid nodules were visible without any post-processing method, while mixed nodule quality was subjectively judged to be of diagnostic quality only in combination with an iterative reconstruction adapted for PCD, as is usually done for ultra-low-dose protocols [27]. But for ULD protocols with conventional CT, lower frequency filter, matrix size of 512, slice thickness of 1.5 mm in addition to the use of denoising algorithms such as iterative reconstruction are recommended [27–29]. It is worth mentioning that conspicuity of ground glass abnormalities under ultra-low-dose conditions improved with use of higher levels of iterative reconstruction, suggesting both improvements in contrast and dose efficiency as well as spatial resolution for PCDs compared to EIDs [3]. Furthermore, low-dose SPCCT imaging on a human volunteer showed acceptable noise quality despite a flux reduction of 89% compared to standard dose conventional CT imaging, a greater matrix size (1024) and a smaller slice thickness (0.25 mm). Nevertheless, SPCCT images demonstrated similar or greater conspicuity and sharpness of the lung structures. Finally, all readers found

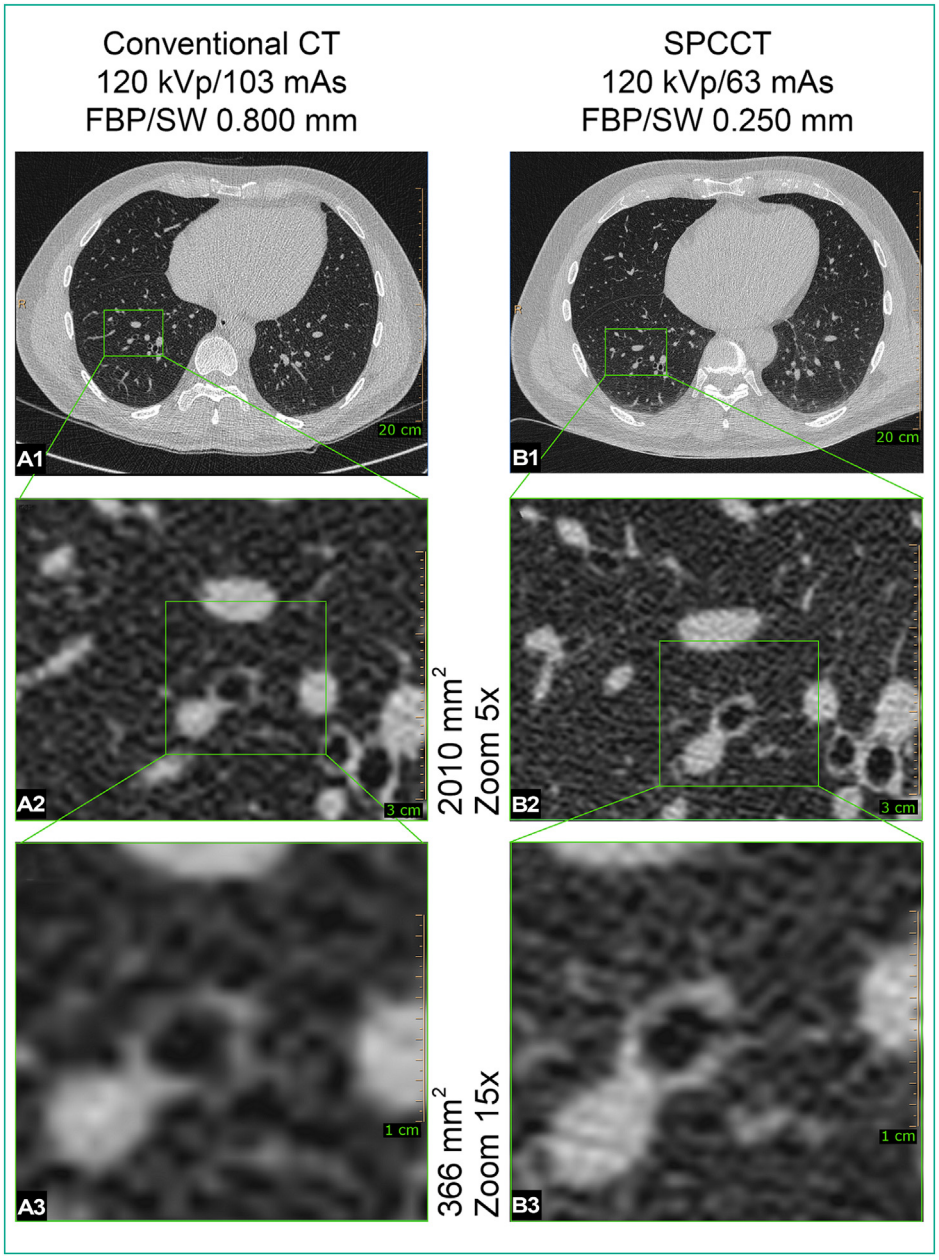

Fig. 5. Human high-resolution spectral photon-counting computed tomography (SPCCT) lung imaging (high matrix, small slice thickness) as compared to a conventional CT scanner: focus on small bronchi (WL −600 HU, WW 1600 HU). Both columns show images of the lungs of the same human subject acquired with a Brilliance 64 CT system (first column) and with the SPCCT system (second column). First row shows a large FOV image of the chest. On the second row, small areas of equivalent dimensions of the right lung base are highlighted. A better definition of bronchial walls on the images obtained with the SPCCT is appreciated. On the third row, two even smaller portions of matching surface are pointed out. While on the Brilliance acquisition only background noise can be seen surrounding the bronchus in the centre, the SPCCT image shows a discontinuity of the bronchus corresponding to the origin of a 0.5 mm diameter bronchiole. Furthermore, the thin walls of the bronchiole can be appreciated as it winds away. Reconstruction parameters: Brilliance 64 – matrix 512; slice thickness, 0.800 mm; kernel, YA. SPCCT – matrix, 1024; slice thickness, 0.250 mm; filter, detailed 2.

a similar overall image quality on low-dose SPCCT images compared to standard conventional CT images without the need for denoising algorithm. Combining these results demonstrates the capability to combine dose efficiency and high spatial resolution to acquire scans with lower radiation dose than with a conventional CT, such as suggested in initial studies [5,26]. This also allows greater radiation dose optimization for other lung applications particularly ones associated with high cumulative dose in young patients with cystic fibrosis or pulmonary arteriovenous malformation [27,30].

In the field of high-resolution lung imaging, two commercial CT systems equipped with EIDs have proposed a high-resolution mode with MTFs in the same range published with SPCCT (20–25 lp/cm at 50%) systems [31,32]. However, these systems cannot offer the several advantages brought by PCDs such as the energy-resolved properties and radiation dose efficiency. This possibly explains the high radiation doses (volume CT dose index 13.65 mGy, mean dose-length product 588.3 mGy.cm) reported in a recent study for high-resolution imaging of lung adenocarcinoma [33].

The present study has limitations. First, an evaluation of the subjective and objective image quality is provided for one only human volunteer. Second, no pathological lesions were found or characterized. Third, the volunteer did not represent the standard patient size limiting the applicability to standard lung imaging practice. Finally, exhaustive evaluation of image quality was out of the scope of the present study opening the way for further investigations.

In conclusion, a large FOV SPCCT prototype paves the way to a technology that not only can fulfil standard clinical requirements with high-resolution and dose efficiency capabilities but also has the potential to overcome current limitations of CT for lung imaging.

Human rights

The authors declare that the work described has been carried out in accordance with the Declaration of Helsinki of the World Medical Association revised in 2013 for experiments involving humans. The local ethics committee approved the study protocol (protocol number: 2018-A02696-49).

Informed consent and volunteer details

The authors declare that this report does not contain any personal information that could lead to the identification of the volunteer.

Funding

This work was supported by European Union Horizon 2020 grant No. 643694 and FLI imaging.

Author contributions

All authors attest that they meet the current International Committee of Medical Journal Editors (ICMJE) criteria for authorship.

Disclosure of interest

Yoad Yagil, Philippe Coulon and Elias Lahoud are employees of Philips Healthcare, the manufacturer of the scanner. The other authors declare that they have no competing interest.

References

[1] Si-Mohamed S, Bar-Ness D, Sigovan M, Cormode DP, Coulon P, Coche E, et al. Review of an initial experience with an experimental spectral photon-counting computed tomography system. Nucl Instrum Methods Phys Res 2017;873:27–35.
[2] Si-Mohamed S, Boussel L, Douek P. Clinical perspectives of spectral photon-counting CT. In: Tagushi K, Blevis I, Iniewski K, editors. Spectral, photon counting computed tomography: technology and applications. Boca Raton, FL, USA: CRC Press; 2020. p. 97–116.
[3] Taguchi K, Iwanczyk JS. Vision 20/20: single photon counting x-ray detectors in medical imaging. Med Phys 2013;40:100901.
[4] Kopp FK, Daerr H, Si-Mohamed S, Sauter AP, Ehn S, Fingerle AA, et al. Evaluation of a preclinical photon-counting CT prototype for pulmonary imaging. Sci Rep 2018;8:17386.
[5] Symons R, Cork TE, Sahbaee P, Fuld MK, Kappler S, Folio LR, et al. Low-dose lung cancer screening with photon-counting CT: a feasibility study. Phys Med Biol 2017;62:202–13.
[6] Bartlett DJ, Koo CW, Bartholmai BJ, Rajendran K, Weaver JM, Halaweish AF, et al. High-resolution chest computed tomography imaging of the lungs: impact of 1024 matrix reconstruction and photon-counting detector computed tomography. Invest Radiol 2019;54:129–37.
[7] Blevis I. X-ray detectors for spectral photon-counting CT. In: Tagushi K, Blevis I, Iniewski K, editors. Spectral, photon counting computed tomography: technology and applications. Boca Raton, FL, USA: CRC Press; 2020. p. 179–91.
[8] Hsieh. Design considerations for photon-counting detectors: connecting detectors characteristics to system performances. In: Tagushi K, Blevis I, Iniewski K, editors. Spectral, photon counting computed tomography: technology and applications. Boca Raton, FL, USA: CRC Press; 2020. p. 326–41.
[9] Si-Mohamed S, Moreau-Triby C, Tylski P, Tatard-Leitman V, Wdowik Q, Boccalini S, et al. Head-to-head comparison of lung perfusion with dual-energy CT and SPECT-CT. Diagn Interv Imaging 2020;101:299–310.
[10] Jamali S, Michoux N, Coche E, Dragean CA. Virtual unenhanced phase with spectral dual-energy CT: is it an alternative to conventional true unenhanced phase for abdominal tissues? Diagn Interv Imaging 2019;100:503–11.
[11] Si-Mohamed S, Cormode DP, Bar-Ness D, Sigovan M, Naha PC, Langlois J-B, et al. Evaluation of spectral photon counting computed tomography K-edge imaging for determination of gold nanoparticle biodistribution in vivo. Nanoscale 2017;9:18246–57.
[12] Cormode DP, Si-Mohamed S, Bar-Ness D, Sigovan M, Naha PC, Balegamire J, et al. Multicolor spectral photon-counting computed tomography: in vivo dual contrast imaging with a high count rate scanner. Sci Rep 2017;7:4784.
[13] Si-Mohamed S, Bar-Ness D, Sigovan M, Tatard-Leitman V, Cormode DP, Naha PC, et al. Multicolor imaging with SPCCT: an in vitro study. Eur Radiol Exp 2018;2:34.
[14] Si-Mohamed S, Thivolet A, Bonnot P-E, Bar-Ness D, Képénékian V, Cormode DP, et al. Improved peritoneal cavity and abdominal organ imaging using a biphasic contrast agent protocol and spectral photon counting computed tomography K-edge imaging. Invest Radiol 2018;53:629–39.
[15] Sigovan M, Si-Mohamed S, Bar-Ness D, Mitchell J, Langlois J-B, Coulon P, et al. Feasibility of improving vascular imaging in the presence of metallic stents using spectral photon counting CT and K-edge imaging. Sci Rep 2019;9:19850.
[16] Steadman R, Herrmann C, Livne A. ChromAIX2: a large area, high count-rate energy-resolving photon counting ASIC for a spectral CT prototype. Nucl Instrum Methods Phys Res 2017;862:18–24.
[17] Bongartz G, Golding SJ, Jurik AG. European guidelines on quality criteria for computed tomography; 2004 [accessed March 26, 2020] http://www.drs.dk/guidelines/ct/quality/htmlindex.htm.
[18] Hatabu H, Hunninghake GM, Richeldi L, Brown KK, Wells AU, Remy-Jardin M, et al. Interstitial lung abnormalities detected incidentally on CT: a Position Paper from the Fleischner Society. Lancet Respir Med 2020;8:726–37.
[19] Lynch DA, Sverzellati N, Travis WD, Brown KK, Colby TV, Galvin JR, et al. Diagnostic criteria for idiopathic pulmonary fibrosis: a Fleischner Society white paper. Lancet Respir Med 2018;6:138–53.
[20] Bankier AA, MacMahon H, Goo JM, Rubin GD, Schaefer-Prokop CM, Naidich DP. Recommendations for measuring pulmonary nodules at CT: a statement from the Fleischner Society. Radiology 2017;285:584–600.
[21] Jalaber C, Lapotre T, Morcet-Delattre T, Ribet F, Jouneau S, Lederlin M. Chest CT in COVID-19 pneumonia: a review of current knowledge. Diagn Interv Imaging 2020;101:431–7.
[22] Neveu S, Saab I, Dangeard S, Bennani S, Tordjman M, Chassagnon G, et al. Incidental diagnosis of Covid-19 pneumonia on chest computed tomography. Diagn Interv Imaging 2020;101:457–61.
[23] Cao L, Wang Z, Gong T, Wang J, Liu J, Jin L, et al. Discriminating between bronchiolar adenoma, adenocarcinoma in situ and minimally invasive adenocarcinoma of the lung with CT. Diagn Interv Imaging 2020;101:831–7.
[24] Leng S, Rajendran K, Gong H, Zhou W, Halaweish AF, Henning A, et al. 150-μm Spatial resolution using photon-counting detector computed tomography technology: technical performance and first patient images. Invest Radiol 2018;53:655–62.
[25] da Silva J, Grönberg F, Cederström B, Persson M, Sjölin M, Alagic Z, et al. Resolution characterization of a silicon-based, photon-counting computed tomography prototype capable of patient scanning. J Med Imaging 2019;6:043502.
[26] Symons R, Pourmorteza A, Sandfort V, Ahlman MA, Cropper T, Mallek M, et al. Feasibility of dose-reduced chest CT with photon-counting detectors: initial results in humans. Radiology 2017;285:980–9.
[27] Greffier J, Boccalini S, Beregi JP, Vlassenbroek A, Vuillod A, Dupuis-Girod S, et al. CT dose optimization for the detection of pulmonary arteriovenous malformation (PAVM): a phantom study. Diagn Interv Imaging 2020;101:289–97.
[28] Beregi JP, Greffier J. Low and ultra-low-dose radiation in CT: opportunities and limitations. Diagn Interv Imaging 2019;100:63–4.
[29] Greffier J, Frandon J, Larbi A, Beregi JP, Pereira F. CT iterative reconstruction algorithms: a task-based image quality assessment. Eur Rad 2020;30:487–500.
[30] Fitton I, Revel M-P, Burgel P-R, Hernigou A, Boussaud V, Guillemain R, et al. Cumulative radiation dose after lung transplantation in patients with cystic fibrosis. Diagn Interv Imaging 2019;100:287–94.
[31] Oostveen LJ, Boedeker KL, Brink M, Prokop M, de Lange F, Sechopoulos I. Physical evaluation of an ultra-high-resolution CT scanner. Eur Radiol 2020;30:2552–60.
[32] Kawashima H, Ichikawa K, Takata T, Nagata H, Hoshika M, Akagi N. Technical note: performance comparison of ultra-high-resolution scan modes of two clinical computed tomography systems. Med Phys 2020;47:488–97.
[33] Yanagawa M, Tsubamoto M, Satoh Y, Hata A, Miyata T, Yoshida Y, et al. Lung adenocarcinoma at CT with 0.25-mm section thickness and a 2048 matrix: high-spatial-resolution imaging for predicting invasiveness. Radiology 2020;297:462–71.